Biomaterials 39 (2015) 155–163

Contents lists available at ScienceDirect

Biomaterials

journal homepage: www.elsevier.com/locate/biomaterials

USPIO-labeled textile materials for non-invasive MR imaging of tissue-engineered vascular grafts

Marianne E. Mertens [a], Sabine Koch [b], Philipp Schuster [c], Jakob Wehner [a], Zhuojun Wu [a, d], Felix Gremse [a], Volkmar Schulz [a], Lisanne Rongen [b], Frederic Wolf [b], Julia Frese [b], Valentine N. Gesché [c], Marc van Zandvoort [d], Petra Mela [b], Stefan Jockenhoevel [b, c, **], Fabian Kiessling [a, *], Twan Lammers [a, e, *]

[a] Dept. of Experimental Molecular Imaging, University Clinic, RWTH Aachen University, Pauwelsstrasse 30, 52074 Aachen, Germany
[b] Dept. of Tissue Engineering & Textile Implants, Applied Medical Engineering, Helmholtz Institute for Biomedical Engineering, RWTH Aachen University, Pauwelsstrasse 20, 52074 Aachen, Germany
[c] Institut für Textiltechnik, RWTH Aachen University, Otto-Blumenthal-Strasse 1, 52074 Aachen, Germany
[d] Institute for Molecular Cardiovascular Research, University Clinic, RWTH Aachen University, Pauwelsstrasse 30, 52074 Aachen, Germany
[e] Dept. of Controlled Drug Delivery, University of Twente, PO Box 217, 7500 AE Enschede, The Netherlands

ARTICLE INFO

Article history:
Received 8 September 2014
Accepted 23 October 2014
Available online 21 November 2014

Keywords:
Tissue engineering
Vascular graft
Textile material
MRI
USPIO

ABSTRACT

Non-invasive imaging might assist in the clinical translation of tissue-engineered vascular grafts (TEVG). It can e.g. be used to facilitate the implantation of TEVG, to longitudinally monitor their localization and function, and to provide non-invasive and quantitative feedback on their remodeling and resorption. We here incorporated ultrasmall superparamagnetic iron oxide (USPIO) nanoparticles into polyvinylidene fluoride (PVDF)-based textile fibers, and used them to prepare imageable tissue-engineered vascular grafts (iTEVG). The USPIO-labeled scaffold materials were molded with a mixture of fibrin, fibroblasts and smooth muscle cells, and then endothelialized in a bioreactor under physiological flow conditions. The resulting grafts could be sensitively detected using T1-, T2- and T2*-weighted MRI, both during bioreactor cultivation and upon surgical implantation into sheep, in which they were used as an arteriovenous shunt between the carotid artery and the jugular vein. In vivo, the iTEVG were shown to be biocompatible and functional. Post-mortem ex vivo analyses provided evidence for efficient endothelialization and for endogenous neo-vascularization within the biohybrid vessel wall. These findings show that labeling polymer-based textile materials with MR contrast agents is straightforward and safe, and they indicate that such theranostic tissue engineering approaches might be highly useful for improving the production, performance, personalization and translation of biohybrid vascular grafts.

1. Introduction

In recent years, significant progress has been made in the development of tissue-engineered materials for cardiovascular purposes, including e.g. blood vessels, heart valves and myocardium [1–8]. However, in spite of the fact that tissue engineering strategies have demonstrated clear potential for improving the biocompatibility and the performance of cardiovascular grafts, the translation of such biohybrid materials into clinically useful products, suitable for implantation into patients, has been slow [9–11]. Among the reasons for this are practical issues, such as difficulties in automated and GMP-based production [12], as well as clinical limitations, related e.g. to the inability to monitor the position and performance of tissue-engineered grafts upon implantation [13].

Materials and methods for non-invasive imaging therefore hold great potential for implementation in tissue engineering, enabling the longitudinal assessment of implant localization, function, maturation, acceptance and remodeling [14]. Consequently, integrating non-invasive imaging in tissue engineering might foster the development of individualized and improved cardiovascular implants, and it might facilitate their clinical translation. Much current interest in this regard is directed toward the use of

* Corresponding authors. Dept. of Experimental Molecular Imaging, Helmholtz Institute for Biomedical Engineering, University Clinic RWTH Aachen University, Pauwelsstrasse 30, 52074 Aachen, Germany. Tel.: +49 (0) 241 8080116; fax: +49 (0) 241 803380116.
** Corresponding author. Dept. of Tissue Engineering and Textile Implants, Applied Medical Engineering, Helmholtz Institute for Biomedical Engineering, RWTH Aachen University, Pauwelsstrasse 20, 52074 Aachen, Germany. Tel.: +49 (0) 241 8089886; fax: +49 (0) 241 803389886.
E-mail addresses: tlammers@ukaachen.de (T. Lammers), fkiessling@ukaachen.de (F. Kiessling), Stefan.Jockenhoevel@ita.rwth-aachen.de (S. Jockenhoevel).

http://dx.doi.org/10.1016/j.biomaterials.2014.10.076
0142-9612/

magnetic resonance imaging (MRI), as it does not involve ionizing radiation, has the capability of imaging tissues at any depth with excellent soft tissue contrast, and has a resolution close to the cellular level. The application of MRI to cardiovascular tissue engineering is of particular interest, since it can provide valuable information on critical parameters such as: i) the morphology and the composition of regenerated vessels; ii) the patency of stent and graft materials; iii) the localization, function and remodeling of the implant material over time; iv) the fate of in vitro colonized cells upon implantation; and v) important (patho-) physiological processes, such as perfusion, inflammation and thrombosis [15–18].

Whereas tissue morphology and vascularization can be assessed without the application of contrast agents, e.g. via relaxometry and time-of-flight (perfusion) measurements, scaffold materials and cells cannot be depicted using conventional MR techniques. The incorporation of MR contrast agents into the cells embedded in tissue-engineered vascular grafts (TEVG) has been shown to be an efficient method for 'indirectly' visualizing the localization and function of TEVG. Ultrasmall superparamagnetic iron oxide (USPIO) nanoparticles are routinely used MR contrast agents [19,20], and have already been employed to label aortic smooth muscle cells (SMC) and endothelial cells (EC) in vascular grafts [21,22]. From a clinical point of view, EC would arguably be the most relevant cellular target to image, in particular if eventually intending to use such constructs in combination with ^{18}F-FDG-based PET imaging, to more easily identify and more accurately quantify vascular inflammation.

Here, to 'directly' visualize vascular grafts in vivo, to monitor their remodeling and resorption, and to facilitate imaging also in case of non-cellularized implants, we developed materials and methods to visualize the scaffold materials themselves. To this end, as exemplified by Fig. 1, USPIO nanoparticles were incorporated into polyvinylidene fluoride (PVDF)-based textile materials, which were knitted into vascular scaffolds. The scaffolds were then molded with a composite of smooth muscle cells (SMC), fibroblasts (FB) and fibrin, and the inner lumen was colonized with endothelial cells (EC) in a bioreactor, to avoid inflammation and thrombus formation. During bioreactor cultivation, the image-guided and tissue-engineered vascular grafts (iTEVG) were monitored using MRI at three different time points. As proof-of-principle for in vivo visualization, they were finally also implanted into sheep, as an arteriovenous shunt between the carotid artery and the jugular vein. USPIO labeling allowed a clear delineation of the textile-based scaffold materials using MRI, and it did not negatively affect the stability, biocompatibility and functionality of the iTEVG. Such theranostic tissue engineering approaches are considered to be relevant both at the preclinical level and in patients, enabling individualized and improved vessel replacement treatments.

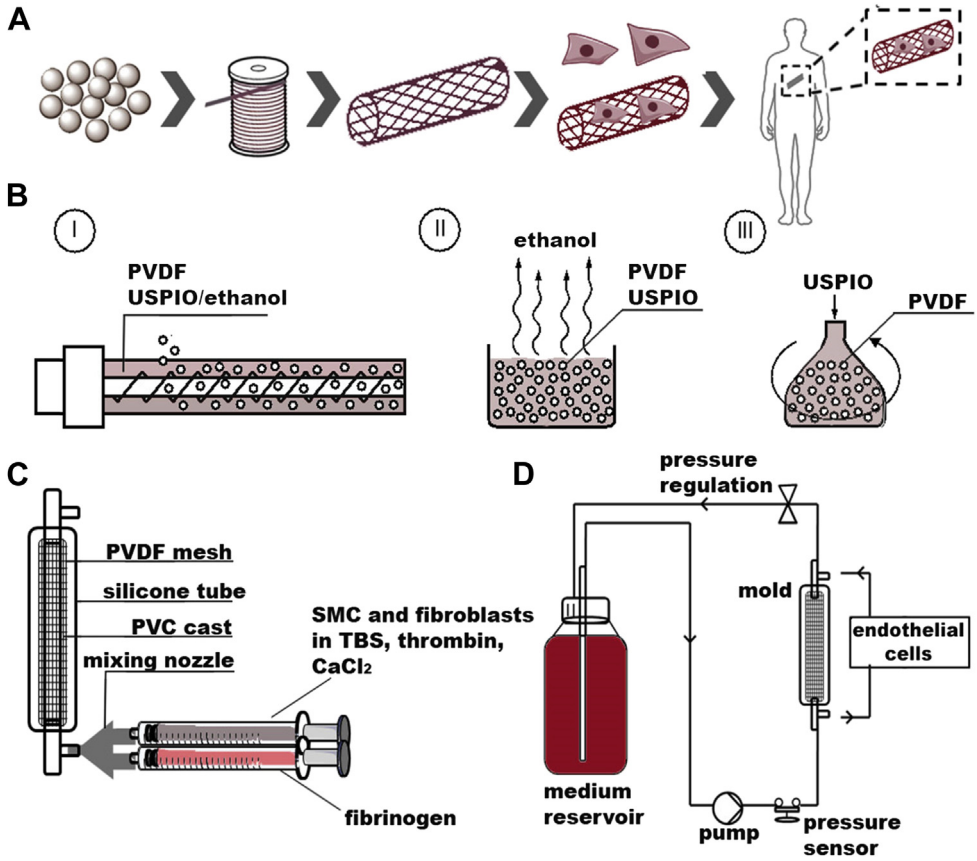

Fig. 1. Production process for USPIO-labeled tissue-engineered vascular grafts. A) PVDF-based polymeric pellets were processed into fibers via melt-spinning and the fibers were further processed into knitted tubular meshes. The meshes were used as scaffolds for the colonization with cells, to produce a biohybrid tissue-engineered vascular graft. B) The incorporation of USPIO nanoparticles into PVDF was carried out in three different ways, in order to find the most suitable procedure for achieving a uniform particle distribution within the matrix. C) An injection molding technique was employed to colonize the PVDF meshes with cells. PVDF meshes were positioned between two cylinders and then covered with the smooth muscle cell/fibroblast/fibrinogen suspension. The polymerization of fibrinogen to fibrin was achieved by using thrombin and calcium chloride. D) Schematic depiction of the bioreactor circuit with pulsatile luminal flow for the mechanical conditioning of the graft. After 7 days, endothelial cells were seeded onto the luminal side of the graft.

2. Materials and methods

2.1. Synthesis of ultrasmall superparamagnetic iron oxide (USPIO) nanoparticles

Ultrasmall superparamagnetic iron oxide (USPIO) nanoparticles were synthesized by co-precipitation of ferrous (Fe^{2+}) and ferric (Fe^{3+}) salts under alkaline aqueous conditions. A modified one-pot synthetic protocol was followed. A stoichiometric ratio of $2Fe^{3+}$: Fe^{2+} (i.e. 12.5 mmol (2.03 g) of $FeCl_3$ and 6.25 mmol (1.24 g) of $FeCl_2.4H_2O$), was dissolved in 190 mL de-ionized water. Afterward, 10 mL of 25% NH_3 were added under vigorous stirring and heated to 80 °C. After 20 min, the particles were washed three times with 30 mL of water and two times with 30 mL of 0.1 m HCl solution by magnetic separation using a rare-earth magnet. Then, the magnetic fluids were dispersed in 25 mL of methanol. The USPIO were sonicated for 20 min prior to centrifugation at 20,000 g for 15 min.

2.2. Synthesis of USPIO-labeled PVDF meshes and characterization

Lyophilized USPIO particles and PVDF granules (Solef®1006 by Solvay Solexis S.A.S., Tavaux, France) were mixed in a rotatory mixing station (Stuart rotator drive STR4, Bibby Scientific Ltd, United Kingdom) at room temperature for 2 h at 30 rpm until USPIO-covered PVDF granules were obtained. USPIO were added in concentrations of 0.05 and 0.2% (w/w). The granule was processed to fibers via melt-spinning using a single-screw lab-melt-spinning machine (Fourné Polymertechnik GmbH, Germany). At process temperatures of 238 °C and take-up speeds of 100 m/min, undrawn multifilament yarns with titers of 175 and 230 dtex comprising 30 single filaments could be manufactured in a stable spinning process. The fibers were characterized by tensile tests (Statimat M, Textechno GmbH, Mönchengladbach, Germany) at standard atmosphere (20 °C, 65% rel. hum.) and by differential scanning calorimetry (TGA/DSC1, Mettler Toledo GmbH, Giessen, Germany). The fibers were further processed into tubular warp-knitted structures on a double raschel warp-knitting machine (DDR 16 EAC/EEC, Karl Mayer Textilmaschinenfabrik GmbH, Obertshausen, Germany).

2.3. Inductively coupled plasma mass spectroscopy analysis

Digestion of the fibers was performed in a closed vessel microwave reaction system (MLS ethos plus, MPV-100/HAT) after addition of 1.5 mL nitric acid (65%) to 1.5 mL hydrogen peroxide and 1 mL of internal standard (rhodium), using 1000 W for 45 min by raising the temperature from 25 °C to 210 °C and left constant at 210 °C for another 15 min. Samples were diluted 1:100 in water. The amount of incorporated iron was determined using a high-resolution sector field inductively coupled plasma mass spectrometer (ICP-MS; Elan-DRCII, Perkin Elmer) equipped with an injector (2.0 mm i.d.). Data was acquired at medium resolution. A Quartz Cyclonic spray chamber equipped with a Meinhard Type A quartz nebulizer was used for sample introduction. The iron content was expressed in grams of iron per kilogram of scaffold material.

2.4. Magnetic resonance imaging in vitro

For MR measurements, the scaffolds were embedded in 10% (w/v) gelatine phantoms and measured in a clinical 3T whole-body MR scanner (Philips Achieva, Best, The Netherlands) using a custom-made small animal solenoid sense-receive mouse coil (40 mm inner diameter and 78 mm bore length; resulting in a 40 mm field of view) (Philips Research Laboratories, Hamburg, Germany). For structural assessment of the scaffolds during colonization, the grafts were transferred within the bioreactor circuit into the MR scanner and measured after 3, 5 and 13 days of cultivation. Transverse (T2) relaxation times were measured in 2D scan mode using a multi-slice, multi-shot spin-echo sequence with a 90° excitation pulse followed by a train of equally spaced 180° refocusing pulses [TR = 1500 ms, TE = 29–584 ms, number of echoes = 20, inter-echo spacing = 29 ms, reconstruction matrix = 112, voxel size = 0.2 × 0.2 mm, slice thickness = 1 mm]. For T2* relaxometry, images at 32 echo times (TE range = 14–168 ms) were acquired by using a multi-shot, multi-slice fast-field gradient-echo sequence [TR = 549 ms, 11 ms interval between two echoes, reconstruction matrix = 192, voxel size = 0.25 × 0.25, slice thickness = 1 mm, 30° flip angle].

T2 and T2* relaxation times (R2 and R2*) were calculated by fitting an exponential curve to the signal amplitudes as a function of the echo time (TE) for each segmented scaffold region using the Imalytics Preclinical Software (Philips Technologie GmbH, Aachen, Germany). The exponential curve includes an offset to account for a signal plateau created by noise or a component with slow signal decay. Furthermore, T1- and T2-weighted images were acquired using a T_1-weighted turbo-spin-echo (TSE) sequence [TR = 500 ms, TE = 20 ms, 0.30 × 0.23 mm voxel size, slice thickness = 1 mm], and a T2-weighted TSE sequence [TR = 1000 ms, TE = 100 ms, 0.25 × 0.25 mm voxel size, slice thickness = 1 mm]. Contrast-to-noise ratios (CNR) were calculated using the formula: $CNR = (S1-S2)/\sigma$, with S1 and S2 being the signal intensities for signal producing structures in the region of interest and σ as the standard deviation of the image noise.

2.5. Biocompatibility tests

Indirect necrosis, proliferation and apoptosis assays were performed to test the influence of the labeled material on cells. Before cell culture use, PVDF-samples were washed and sterilized using low-temperature hydrogen peroxide gas plasma (STERRAD® 100S Sterilization System; Ethicon GmbH, Hamburg, Germany). An evaporation time of at least 10 days was conducted to avoid cell irritation caused by the plasma. Afterward the PVDF fibers labeled with 0.2% (w/w) USPIO (microfilament diameter of 60.8 μm and 39.9 μm) were incubated in medium (1.5 cm^2/mL medium); SMC/FB: DMEM, Low Glucose, GlutaMAX™, Pyruvate, Gibco® plus 10% FBS Fetal Bovine Serum, PAA Cölbe, Germany; EC: Endothelial Basal Medium and Medium Supplement (PAA, Cölbe, Germany) plus 1% Glutamax (Invitrogen) for 72 h at 37 °C to prepare the test medium. Ovine SMC/fibroblasts (5×10^3 cells/well) and endothelial cells (10×10^3 cells/well) were seeded in a 96-well plate and cultivated for 24 h before treatment. Culture medium was removed and the wells washed with Dulbecco's Phosphate Buffered Saline PBS (1×) without Ca & Mg (PAA, Cölbe, Germany) before the test medium was added. Three different assays to test necrosis (ToxiLight® BioAssay, Lonza), apoptosis (Caspase-Glo® 3/7 assay, Promega) and proliferation (Cell Proliferation Kit II XTT, Promega) were performed after 2, 4 and 6 days of incubation according to the manufactures protocols. As a positive control for necrosis the cells were lysed before measurement with ToxiLight® Lysis Reagent (Lonza). As a positive control for caspase activation cells were exposed to UV light for 4 min. For proliferation assessment cells treated with medium without FBS served as negative control. The emitted light was measured with a multi-plate reader (Infinite M200, TECAN).

2.6. Cell isolation and culture

Endothelial cells and a mixed population of SMC/FB were obtained from ovine carotid artery using previously established procedures [23]. SMC/FB were cultured in Dulbecco's modified Eagle's medium (Invitrogen, Darmstadt, Germany) supplemented with 10% fetal calf serum (PAA, Cölbe, Germany). EC were treated with "Endothelial Basal Medium and Endothelial Medium Supplement" (PAA, Cölbe, Germany). The cells were serially passaged using 0.25% trypsin/0.02% EDTA (PAA, Cölbe, Germany). Cells were maintained in culture at 37 °C in a humidified incubator (5% CO_2 and 95% humidity). Prior to graft synthesis, cell phenotype was verified by testing á-smooth muscle actin (á-SMA) presence and absence of von Willebrand factor (vWF) for SMC/FB and positive vWF staining for EC.

2.7. Fibrin synthesis

Fibrinogen (Calbiochem®) was dissolved in ultrapure water and dialyzed overnight against Tris-buffered saline (TBS; pH 7.4; Schnelldorf, Germany) using a dialysis membrane (Novodirect, Kehl, Germany) with a molecular weight cut-off of 6–8 kDa. Subsequent to sterile filtration, the fibrinogen concentration was optically determined by measuring the absorbance at 280 nm using a spectrophotometer (Tecan Infinite M200; Tecan, Crailsheim, Germany) and adjusted to 10 mg/mL with sterile TBS. The entire tissue-engineered graft (4.0 mL total volume) was composed of 2.0 mL fibrinogen solution (10 mg/mL), 1.4 mL TBS-containing carotid artery-derived cells (12.5×10^6 cells/mL), 300 mL 50 mM $CaCl_2$ (Sigma, Schnelldorf, Germany), and 300 mL thrombin solution (40 U/mL, Sigma, Schnelldorf, Germany).

2.8. Graft molding and cell seeding

Vascular composite grafts were molded as described previously [23]. Each PVDF mesh was positioned over an inner cylinder of the mold before insertion into the outer cylinder. Subsequently, the annular space between the inner and outer cylinders of the mold was filled with the cell/fibrin gel suspension (12.5×10^6 cells/mL), which provided a uniform wall thickness throughout the graft. After 45 min, complete polymerization was achieved. The inner casting cylinder was removed, and the graft was maintained in the outer cylinder. Subsequently, the graft was connected to a bioreactor system and transferred to an incubator at 37 °C and 5% CO_2 for mechanical conditioning. Medium flow through the graft was gradually increased from 20 mL/min to 100 mL/min over a 14-day conditioning period, at physiological pressure conditions (120 mmHg systolic pressure, 80 mmHg diastolic pressure). The culture medium used in the bioreactor system consisted of DMEM with 10% FCS and 1% antibiotic-antimycotic solution (PAA, Cölbe, Germany), and it was changed once per week under sterile conditions. L-ascorbic acid-2-phosphate (1.0 mM; Sigma, Schnelldorf, Germany) was added to increase collagen synthesis. Fibrin degradation was controlled by supplementation of the medium with 0.16 mg/ml Cyklokapron® injection solution (Pfizer, Berlin, Germany).

2.9. Histology

Carnoy-fixed and paraffin-embedded tissue-engineered grafts were sectioned perpendicular to their lumen, at a thickness of 3 mm. H&E staining allowed for analysis of overall tissue preservation. Gomori's trichrome staining (0.6% Chromotrop 2R, 0.3% Fast Green FCF, 0.7% phosphotungstic acid and 1% acetic acid) was done for tissue development analysis. Sections were viewed using a routine bright field microscope (AxioImager D1; Carl Zeiss GmbH, Jena, Germany). Images were acquired using a digital color camera (AxioCam MRc; Carl Zeiss GmbH, Jena, Germany). Immunofluorescence stainings were performed using a primary antibody against the proliferation marker Ki67, which was incubated for 60 min at room temperature, followed by secondary antibody staining and nuclear counterstaining using Hoechst. Collagen autofluorescence was imaged in the green channel. Stained sections were

examined using a Zeiss Axio Imager M2. For quantitative analysis of collagen synthesis, hydroxyproline content in dried grafts was determined. A standard curve was generated using known amounts of trans-4-hydroxy-L-proline (Sigma, Schnelldorf, Germany).

2.10. In vivo evaluation

The animal experiment was approved by the governmental review committee on animal care (84-02.04.2012.A351). Two healthy adult sheep (Rhönschaf breed) were used, for the in vivo evaluation of 1 non-labeled and 1 USPIO-labeled (0.2% (w/w)) biohybrid vascular graft. The grafts were implanted as arteriovenous shunts between the carotid artery and the jugular vein. MR imaging was carried out under Xylazin/Atropin anesthesia, using a clinical 3T MR scanner, in combination with a PMS SENSE Head Spine Coil (Philips Research Laboratories, Hamburg, Germany). Grafts were visualized using a proton-weighted multi-shot, multi-slice fast-field gradient-echo (FFE) sequence [TE = 4 ms, TR = 1000 ms, FA = 60°, FOV = 60 × 22 × 60 mm], and patency was evaluated using a 3D T1-weighted FFE phase-contrast angiography (PCA) [TE = 4 ms, TR = 10 ms, FA = 15°, FOV = 68 × 300 × 150 mm].

2.11. Ex vivo evaluation

The explanted part of the graft was incubated with SYTO 61 for 45 min (5 nM, Invitrogen) and subsequently embedded in 1% agarose. Two-photon laser scanning microscopy (TPLSM) imaging was performed using an Olympus FV1000MPE multiphoton microscopy system (Mai Tai DeepSee pulsed Ti:Sapphire laser with 140 fs pulsewidth at an excitation wavelength of 800 nm and a 25× water dipping objective (Numerical Aperture (NA) = 1.05, Working Distance (WD) = 2 mm)). Three internal photon multiplier tubes were used to detect the fluorescence signals, and filters were adjusted to the corresponding spectra: 390–480 nM for collagen second harmonic generation, 495–540 for scaffold autofluorescence, and 595–650 for SYTO 61. TPLSM images were analyzed using Imaris software (Bitplane). Electron microscopy was performed at the core facility for electron microscopy at RWTH Aachen University Clinic. For scanning electron microscopy (SEM), the grafts were fixed on SEM stubs, sputter-coated with gold, and analyzed using a field emission SEM microscope (ESEM XL 30 FEG, FEI, Philips, Eindhoven, The Netherlands) in a high-vacuum environment. For transmission electron microscopy (TEM), the grafts were embedded in Epon, polymerized 8 h at 37 °C, 56 h at 60 °C, cut into 70–100 nm thick slices, and analyzed using TEM microscope (EM 400 T, Philips, Eindhoven, The Netherlands).

2.12. Statistical analysis

All results are presented as average ± standard deviation. For the comparison of R2, R2* and CNR values, one-way ANOVA with Bonferroni post-hoc correction was performed. Correlation coefficients (Pearson) and P values (two-tailed) were calculated using the GraphPad Software (version 4.0). $P < 0.05$ was considered to represent statistical significance.

3. Results

3.1. Synthesis and characterization of USPIO-labeled PVDF fibers

The incorporation of USPIO nanoparticles into the PVDF-based polymeric material was carried out in three different ways, to identify the most suitable procedure for achieving efficient and uniform particle distribution in the matrix (Fig. 1B). In the first approach, a twin-screw extruder was used to compound USPIO and PVDF at temperatures above the melting point of PVDF. Since introducing small amounts of lyophilized USPIO into the twin-screw channel proved to be difficult, a liquid metering system was used. Ethanol or 1,2-butanediol were used as dispersants, but both started to seethe before reaching the twin-screw channel, resulting in inefficient USPIO incorporation. In the second approach, USPIO were dispersed in ethanol and mixed with PVDF granules in an ultrasonic bath for 5 min at RT. The batch was then stored at 90 °C under a fume hood until the ethanol completely evaporated and USPIO-covered PVDF granules remained. These granules could be successfully processed into fibers via melt-spinning. In the third and most straightforward approach, lyophilized USPIO nanoparticles were directly mixed with PVDF granules in a rotatory mixing station at 30 rpm for 2 h at RT, obtaining USPIO-labeled PVDF granules which could also be successfully processed into fibers via melt-spinning.

The latter of the above approaches was found to be the most appropriate one in terms of practicality and process stability, and was therefore used to produce PVDF granules embedding different amount of USPIO, i.e. 0.05 and 0.2% (w/w) (Fig. 2A, top row). These granules, as well as USPIO-free control PVDF granules, were processed into fibers via melt-spinning, using a single-screw lab-melt-spinning machine. Single filaments could be manufactured in a stable spinning process (Fig. 2A, middle row). The final iron content in the fibers was confirmed by inductively coupled plasma mass spectrometry (ICP-MS), and was found to be 0.6 ± 0.1 mg Fe/g for fibers with 0.05% (w/w) USPIO and 2.0 ± 0.3 mg Fe/g for fibers with 0.2% (w/w) USPIO.

The as-spun fibers were characterized by tensile tests and differential scanning calorimetry (DSC). Interestingly, it was found that tensile strength slightly increased with USPIO content (Fig. 2C). This correlated with a slight increase of the enthalpy of fusion: 38.4 J/g for non-labeled fibers vs. 42.3 J/g for fibers with 0.05% (w/w) USPIO and 45.2 J/g for fibers with 0.2% (w/w) USPIO. This hints towards a higher crystallinity of the PVDF yarn with rising USPIO content, which can likely be attributed to the nucleating effect of the nanoparticles.

Subsequently, the labeled fibers were visualized using MRI (Fig. 2A, bottom row), and the corresponding R2 and R2* values were calculated on the basis of relaxometry measurements (Fig. 2B). A significant increase in R2 and R2* vs. unlabeled scaffolds could be detected at a concentration of 0.2% (w/w) USPIO (R2: $p < 0.01$, $R^2 = 0.9223$; R2*: $p < 0.001$, $R^2 = 0.9548$) and a clear improvement of visibility could be achieved upon USPIO incorporation.

For initial biocompatibility testing (i.e. to assess whether any potentially toxic compounds are released from the labeled fibers), necrosis, proliferation and apoptosis assays were performed. To this end, the fibers were exposed to cell culture medium for 72 h, and the pre-conditioned medium was used for the cultivation of SMC/FB and EC. Fibers with a microfilament diameter of 60.8 μm (30 microfilaments; resulting in a surface of 5733 mm^2/m) and 38.9 μm (30 microfilaments; resulting in a total surface of 3673 mm^2/m) were tested. As shown in Fig. 2D, pre-incubation with neither of these two materials resulted in cytotoxic effects.

3.2. Preparation and in vitro evaluation of tissue-engineered vascular grafts

After confirming the stability, MR visibility and biocompatibility of the labeled fibers, they were processed into tubular warp-knitted structures on a double raschel warp-knitting machine (Fig. 3A). A macroporous mesh design was selected, in order to fulfill the elasticity requirements needed for application as a TEVG. The resulting labeled meshes were characterized using MRI, demonstrating a clear improvement of visibility in T1, T2 and T2* -weighted images (Fig. 3B), and rendering significant increases in R2 and R2* relaxation rates and contrast-to-noise ratios (CNR) as compared to non-labeled meshes (R2: $p < 0.001$, $R^2 = 0.9522$; R2*: $p < 0.001$, $R^2 = 0.9295$, CNR T2: $p < 0.05$, $R^2 = 0.6976$; CNR T2*: $p < 0.0001$, $R^2 = 0.9373$; Fig. 3D–E). Fig. 3C shows that 3-dimensional rendering of the labeled mesh materials enabled a highly detailed visualization of scaffold size and structure.

Subsequently, the USPIO-labeled scaffolds were molded with cell-seeded fibrin to produce image-guided and tissue-engineered iTEVG (Fig. 4). SMC/FB and EC were isolated from the carotid artery of sheep, and expanded in vitro. Fibrin is a major structural protein involved in wound healing, and possesses a nanofibrous network structure which enables the gentle embedding of cells, high cell seeding efficiency and homogenous cell distribution [23].

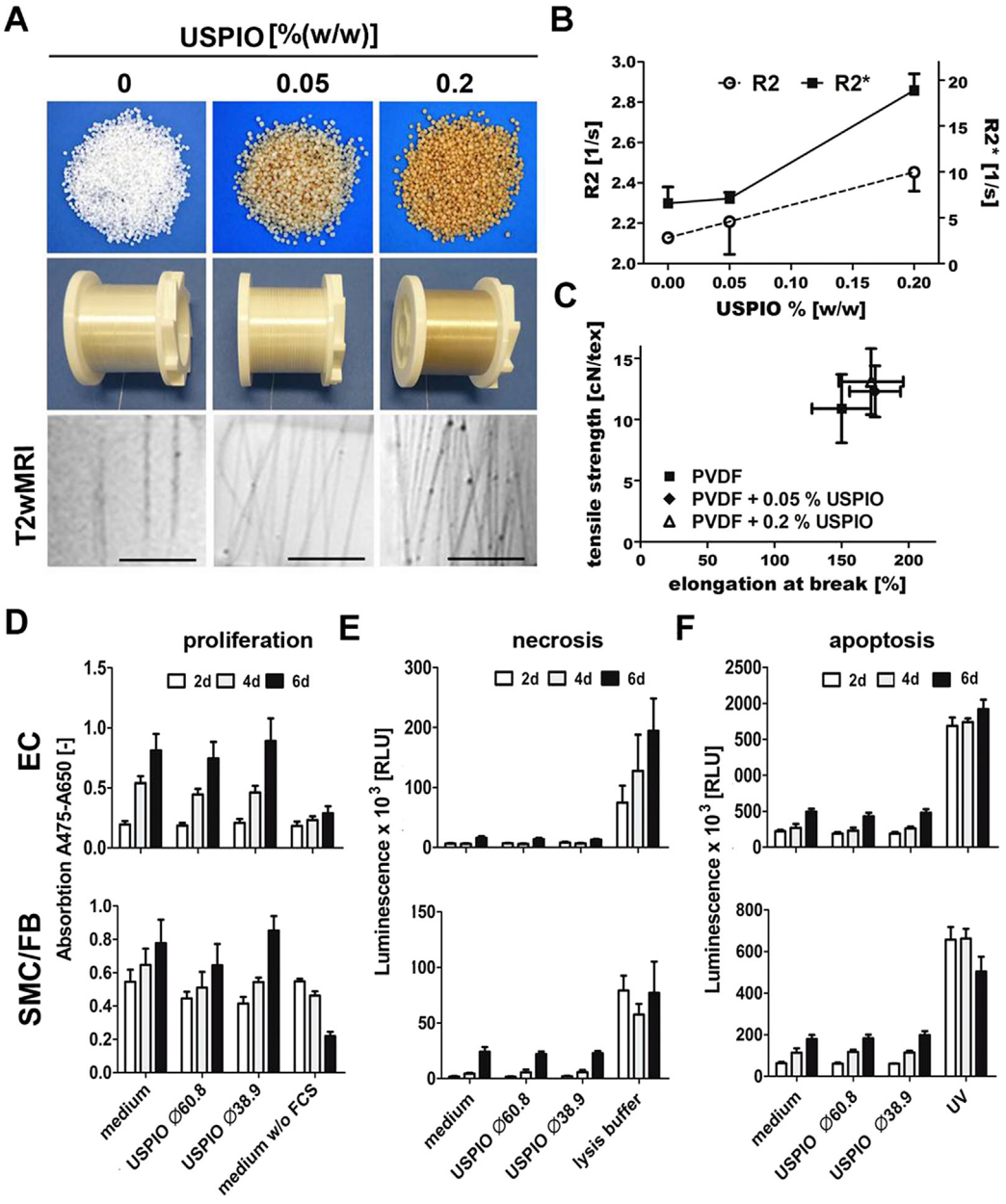

Fig. 2. Synthesis, MR analysis, stability and biocompatibility evaluation of USPIO-labeled PVDF fibers. A) USPIO-labeled PVDF pellets (top) and fibers (middle) containing 0, 0.05 and 0.2% (w/w) of iron oxide nanoparticles. Visualization of the labeled fibers in T2-weighted MRI is shown in the bottom panels. Scale bar = 5 mm. B) Quantitative R2 and R2* relaxometry analysis. C) Mechanical strength testing of labeled fibers (175 dtex), indicating a slight increase in tensile strength upon USPIO incorporation. D–F) Biocompatibility was evaluated by incubating fibers with a microfilament diameter of 60.8 μm and 39.9 μm for 72 h with cell culture medium, and by subsequently using this pre-conditioned medium for the cultivation of smooth muscle cells (SMC)/Fibroblasts (FB) and endothelial cells (EC). D–F) Assessment of proliferation (XTT assay; D), necrosis (Toxilight assay; E) and apoptosis (Caspase assay; F). No apparent toxicity could be observed.

A two-piston dual-syringe system enabled the simultaneous injection and gentle mixing of the soluble fibrin precursor fibrinogen with a buffer suspension containing SMC, FB, thrombin and calcium chloride, which together induce polymerization within the mold (Fig. 1C). After 45 min, when the fibrin was completely polymerized, the graft was connected to a bioreactor system for nutritional supply and mechanical stimulation, and it was transferred into an incubator for further cultivation and conditioning (Fig. 1D). After 7 days of bioreactor cultivation, autologous ovine endothelial cells were seeded on the luminal side of the graft, and they were conditioned under physiological flow conditions for another 8 days.

The shape, patency, contrast properties and relaxation rates of the iTEVG were monitored at three different time points during bioreactor cultivation (Fig. 4B). At each time point, the grafts could be successfully visualized in T1, T2 and T2* -weighted MRI (Fig. 4C), and a clear increase in relaxation rates and CNR could be demonstrated for grafts functionalized with 0.2% (w/w) USPIO (Fig. 4D–E: 13*d* R2/R2*: $p < 0.05$, R^2 (R2) = 0.8478, R^2 (R2*) = 0.7000, 13*d* CNR T2/T2*: $p < 0.01$, R^2 (CNR T2) = 0.9233, R^2 (CNR T2*) = 0.8683). Since relaxation rates remained constant during bioreactor cultivation, it was reasoned that USPIO incorporation is stable even under physiological flow conditions. Three-dimensional rendering provided feedback on the intactness of the iTEVG, as well as on the

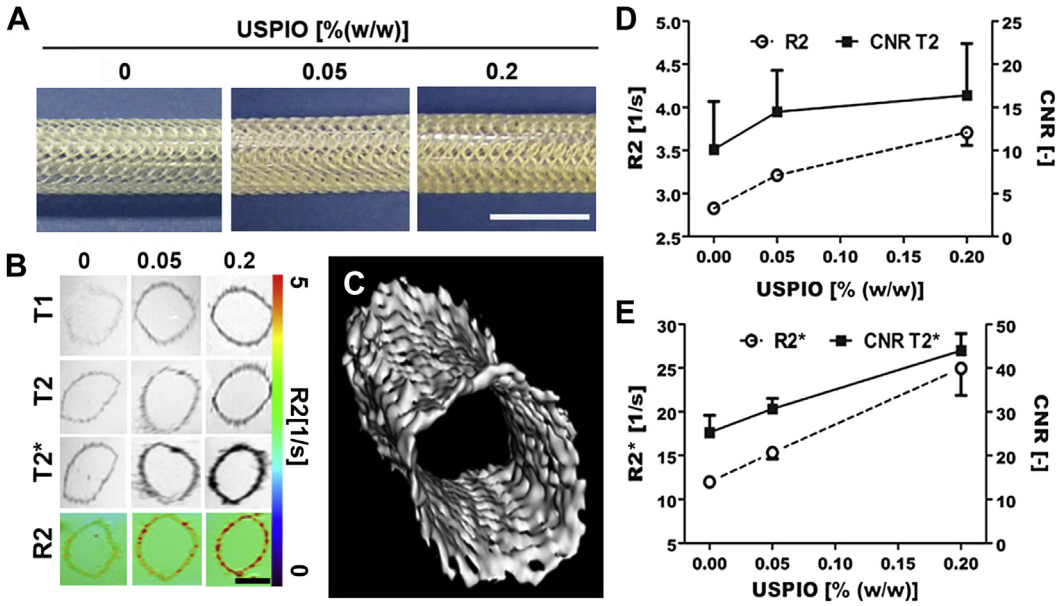

Fig. 3. MR characterization of labeled and non-labeled PVDF meshes. A) PVDF meshes with 0–0.2% (w/w) incorporated USPIO nanoparticles. Scale bar = 1 cm. B) MR visualization using T1, T2 and T2* MRI and R2* mapping (left). Scale bar = 5 mm. C) 3D rendering of a labeled graft. D, E) Quantitative analysis of the relaxation rate and contrast-to-noise ratios in T2 (D) and T2* (E) MRI. Labeled scaffolds presented with strong hypointense contrast, which corresponded to an increase in R2 and in particular in R2* relaxation rates.

presence of partially collapsed regions (Fig. 4B). This image-guided procedure consequently conveys important information on production, processing and cultivation parameters, and enables real-time quality control of tissue-engineered materials prior to implantation. Histological analysis of the bioreactor-cultivated vascular grafts confirmed homogenous colonization and integration of the PVDF meshes, and demonstrated that USPIO labeling did not negatively affect vessel formation (Fig. 4F).

3.3. *In vivo evaluation of USPIO-labeled and tissue-engineered vascular grafts*

Finally, proof-of-principle for monitoring the in vivo localization and function of iTEVG was provided. To this end, they were implanted in sheep, as an arteriovenous shunt between the carotid artery and the jugular vein. As shown in Fig. 5A–B, the labeled grafts could be sensitively visualized and accurately localized using proton density-weighted MRI, whereas non-labeled scaffolds could not be delineated. The patency of the labeled graft was confirmed for up to 2 months post implantation, using phase-contrast angiography (PCA; Fig. 5C).

Post-mortem ex vivo analyses using transmission and scanning electron microscopy demonstrated the formation of a confluent and smooth endothelial lining on the luminal side of the graft, the development of 'endogenous' neovessels within the graft, and a proper integration of the PVDF-based scaffold material within the extracellular matrix (Fig. 5D–G). These findings were confirmed using two-photon laser scanning microscopy of explanted graft material (Fig. 5H–I). Importantly, in these post-mortem analyses, no indications hinting toward tissue necrosis, calcification and/or infection were observed. This is consistent with previous findings, demonstrating similar or enhanced biocompatibility of TEVG in comparison to clinically used GoreTex prostheses [23].

4. Discussion

Our findings show that the incorporation of USPIO nanoparticles within PVDF-based textile materials allows a clear delineation of tissue-engineered vascular grafts in T1, T2 and T2* -weighted MRI, without negatively affecting their stability, biocompatibility and performance. During bioreactor cultivation, non-invasive imaging can provide real-time information on the intactness and the patency of TEVG, thereby enabling non-destructive quality control prior to implantation (Figs. 2–4). It furthermore significantly facilitates the localization of TEVG upon in vivo implantation (Fig. 5), and might therefore be highly useful when monitoring vascular graft inflammation using hybrid PET-MRI. Implantation into sheep confirmed the visibility, the biocompatibility and the functionality of the iTEVG (Fig. 5).

Regarding the application and the clinical translation of iTEVG, several issues have to be taken into account. For instance, the majority of biomaterials employed for (cardiovascular) tissue engineering purposes are based on natural or synthetic polymers [24,25], which are very difficult to visualize using conventional imaging techniques. To visualize the location of implanted materials, it is therefore necessary to establish means to facilitate their in vivo identification. The functionality of TEVG is generally assessed using MRI, computed tomography (CT) or ultrasound (US) angiography, which provide feedback on potential narrowing of the graft lumen, but which do not convey information on potential reasons. The direct visualization of the scaffold material using MRI, on the other hand, provides valuable feedback on the integrity and morphology of the implants, it helps to identify collapsed regions and vascular leakages, and it may thereby facilitate decision-making with respect to pharmacological and/or surgical interventions.

Biomaterials used for tissue engineering purposes are furthermore often biodegradable, and undergo resorption and remodeling in vivo. As recently demonstrated for USPIO-labeled collagen matrices [26], non-invasive MR imaging can also be employed to assess the degradation kinetics of tissue-engineered implant materials, and it can help to tailor the material characteristics and optimize them for different sites of implantation and/or different types of applications. By e.g. using polylactide instead of PVDF, similar strategies can be envisioned for visualizing and quantifying the resorption of TEVG.

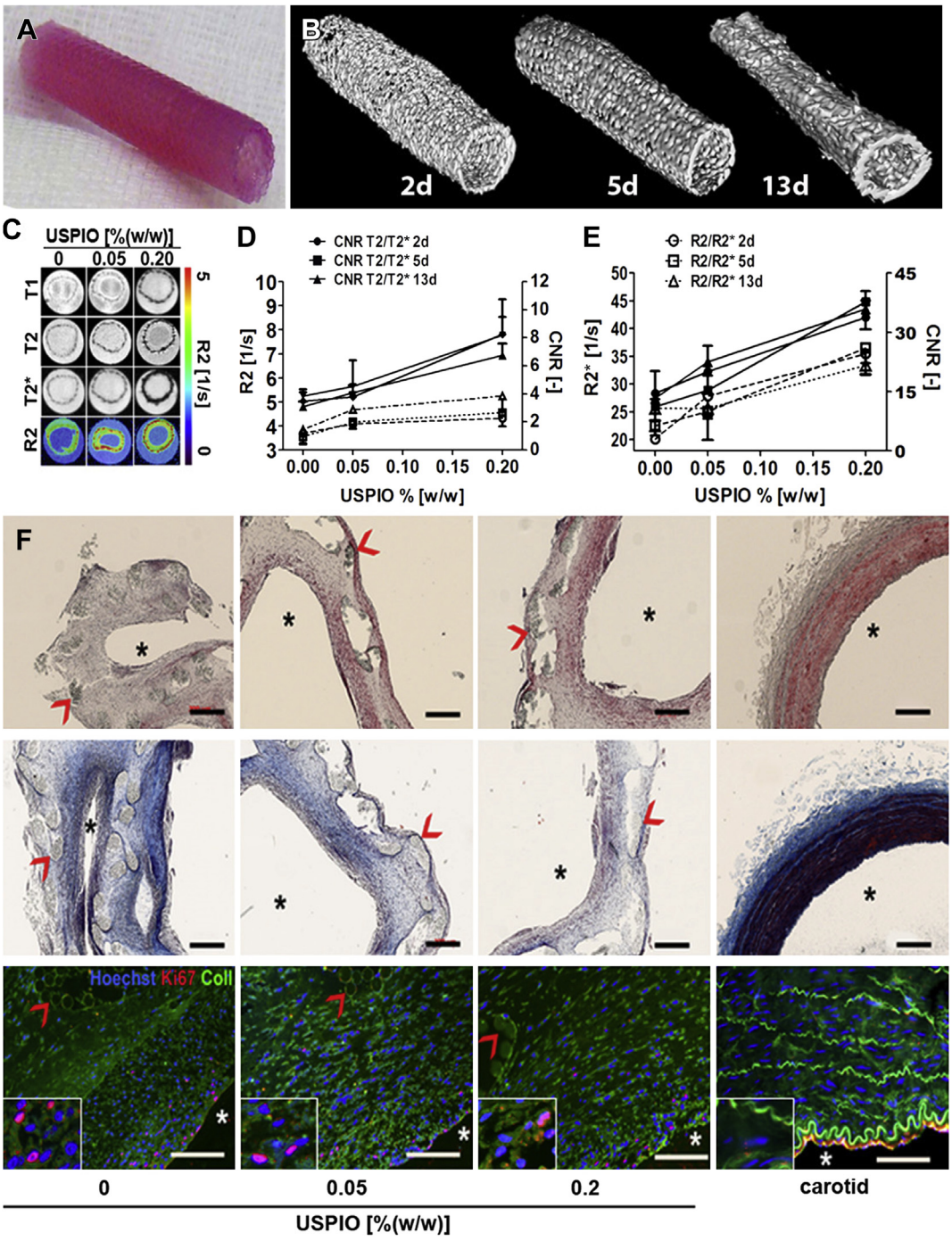

Fig. 4. MR imaging and histological analysis of USPIO-labeled and tissue-engineered vascular grafts. A) Photograph of a tissue-engineered vascular graft after 14-days of bioreactor cultivation. B) Longitudinal 3D MRI rendering of a vascular graft (0.2% USPIO) after 2, 5 and 13 days of cultivation. C) Exemplary T1, T2 and T2* -weighted MR images and R2 mapping after 5 days of cultivation. D, E) R2 and CNR in T2 (D) and T2* (E) images after 2, 5 and 13 days of bioreactor cultivation. The shape and patency of the labeled grafts could be accurately assessed, and contrast and relaxation rates were significantly increased in grafts labeled with 0.2% (w/w) USPIO. F) Hematoxylin and eosin (top), Gomori's trichrom (middle) and Ki67 (bottom) stainings of non-labeled and USPIO-labeled tissue-engineered vascular grafts. A freshly explanted sheep carotid artery was used as positive control. Asterisks indicate the vessel lumen and arrows highlight the PVDF-based scaffold material.

In summary, we here show that USPIO nanoparticles can be efficiently embedded within textile-based scaffold materials. In addition, we provide proof-of-principle for the theranostic use of image-guided and tissue-engineered vascular grafts (iTEVG) in a clinically relevant large animal model. These findings are considered to be important for individualizing and improving vessel replacement therapies, in particular if the iTEVG can be employed in settings allowing for hybrid PET-MRI, using ^{18}F-FDG to monitor macrophage activity and implant-associated inflammation. Combining anatomical and functional MR information (on graft implantation, localization, perfusion and remodeling) with molecular PET information (on vascular inflammation and on the efficacy of anti-inflammatory drug treatment) is therefore expected to be highly useful for facilitating the clinical translation of TEVG.

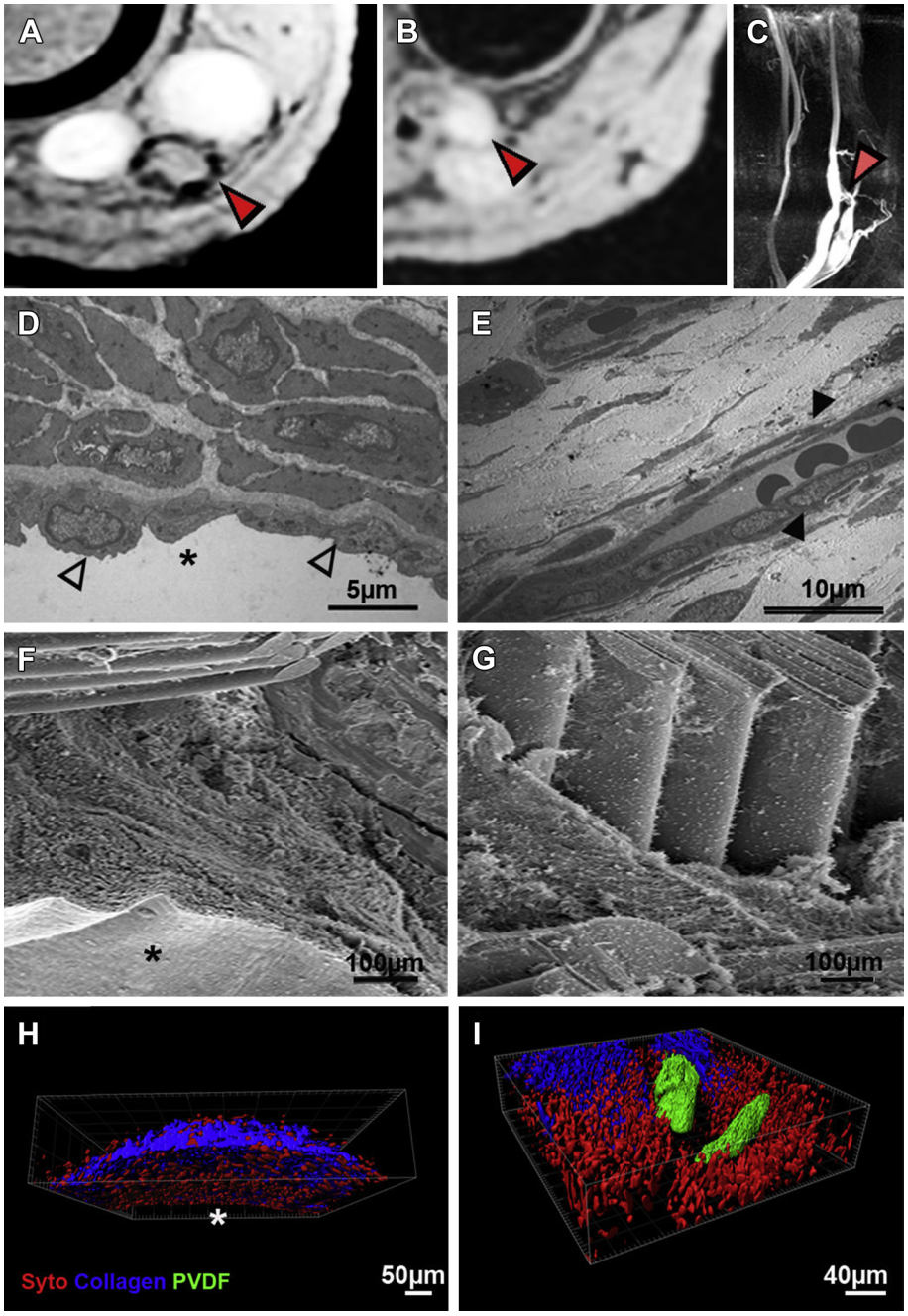

Fig. 5. In vivo imaging and ex vivo validation of a USPIO-labeled arteriovenous shunt. A, B) Proton density-weighted MRI of a USPIO-labeled (A) and a non-labeled (B) vascular graft upon implantation as an arteriovenous shunt in sheep. Red arrowheads indicate the grafts. C) Phase-contrast angiography (PCA) of a USPIO-labeled vascular graft. The shunt could be clearly delineated in vivo and patency could be confirmed. D, E) Transmission electron microscopy (TEM) imaging of tissue-engineered endothelium (D: open arrowheads indicate endothelial layer, asterisk indicates the shunt lumen) and endogenously formed neovessels within the regenerated tissue (E: closed arrowheads). F, G) Scanning electron microscopy (SEM), showing the vessel wall (F: asterisk indicates the lumen) and exemplifying extracellular matrix (ECM) formation around the PVDF mesh (G). H, I) Two-photon laser scanning microscopy (TPLSM) analysis, confirming proper cellular colonization on the luminal side of the graft (SYTO-staining; H) and proper integration of the PVDF-based scaffold material in the interior of the graft (I). (For interpretation of the references to color in this figure legend, the reader is referred to the web version of this article.)

Acknowledgments

The authors gratefully acknowledge technical support by Anne Rix and Diana Möckel, and by the core facilities for electron microscopy and multi-photon microscopy at the Interdisciplinary Center for Clinical Research (IZKF) at RWTH Aachen University. This work was funded by NRW/EU-Ziel 2-Programm (EFRE) 2007–2013: "Entwicklung und Bildgebung patientenoptimierter Implantate" the Helmholtz-Society Portfolio Grant "Technologie und Medizin: Multimodale Bildgebung zur Aufklärung des In-vivo-Verhaltens von polymeren Biomaterialien", the European Research Council (ERC Starting Grant 309495: NeoNaNo), and the ERS Boost Fund Program at RWTH Aachen University.

References

[1] Hoerstrup SP, Kadner A, Melnitchouk S, Trojan A, Eid K, Tracy J, et al. Tissue engineering of functional trileaflet heart valves from human marrow stromal cells. Circulation 2002;106:I143–50.

[2] Hoerstrup SP, Mrcs IC, Lachat M, Schoen FJ, Jenni R, Leschka S, et al. Functional growth in tissue-engineered living, vascular grafts. Circulation 2006;114: I159–66.
[3] Morritt AN, Bortolott SK, Dilley RJ, Han X, Kompa AR, McCombe D, et al. Cardiac tissue engineering in an in vivo vascularized chamber. Circulation 2007;115:353–60.
[4] Cleary MA, Geiger E, Grady C, Best C, Naito Y, Breuer C. Vascular tissue engineering: the next generation. Trends Mol Med 2012;18:394–404.
[5] Chan V, Raman R, Cvetkovic C, Bashir R. Enabling microscale and nanoscale approaches for bioengineered cardiac Tissue. ACS Nano 2013;7:1830–7.
[6] Sekine H, Shimizu T, Sakaguchi K, Dobashi I, Wada M, Yamato M, et al. In vitro fabrication of functional three-dimensional tissues with perfusable blood vessels. Nat Commun 2013;4:1399.
[7] Driessen-Mol A, Emmert MY, Dijkman PE, Frese L, Sanders B, Weber B, et al. Transcatheter implantation of homologous "off-the-shelf" tissue-engineered heart valves with self-repair capacity: long-term functionality and rapid in vivo remodeling in sheep. J Am Coll Cardiol 2014;63:1320–9.
[8] Mack M. Progress toward tissue-engineered heart valves. J Am Coll Cardiol 2014;63:1330–1.
[9] Shastri VP. In vivo engineering of tissues: biological considerations, challenges, strategies, and future directions. Adv Mater 2009;21:3246–54.
[10] Hollister SJ. Scaffold design and manufacturing: from concept to clinic. Adv Mater 2009;21:3330–42.
[11] Pashuck ET, Stevens MM. Designing regenerative biomaterial therapies for the clinic. Sci Transl Med 2012;4. 160sr4.
[12] Langer RS, Vacanti JP. Tissue engineering: the challenges ahead. Sci Am 1999;280:86–9.
[13] Appel AA, Anastasio MA, Larson JC, Brey EM. Imaging challenges in biomaterials and tissue engineering. Biomaterials 2013;34:6615–30.
[14] Advancing tissue science and engineering: a foundation for the future. A multi-agency strategic plan. Tissue Eng 2007;13:2825.
[15] Neu CP, Arastu HF, Curtiss S, Reddi AH. Characterization of engineered tissue construct mechanical function by magnetic resonance imaging. J Tissue Eng Regen Med 2009;3:477–85.
[16] Towner RA, Smith N, Asano Y, He T, Doblas S, Saunders D, et al. Molecular magnetic resonance imaging approaches used to aid in the understanding of angiogenesis in vivo: implications for tissue engineering. Tissue Eng Part A 2010;16:357–64.
[17] Poirier-Quinot M, Frasca G, Wilhelm C, Luciani N, Ginefri JC, Darrasse L, et al. High-resolution 1.5-tesla magnetic resonance imaging for tissue-engineered constructs: a noninvasive tool to assess three-dimensional scaffold architecture and cell seeding. Tissue Eng Part C Methods 2010;16:185–200.
[18] Xu H, Othman SF, Magin RL. Monitoring tissue engineering using magnetic resonance imaging. J Biosci Bioeng 2008;106:515–27.
[19] Gutpa AK, Gupta M. Synthesis and surface engineering of iron oxide nanoparticles for biomedical applications. Biomaterials 2005;18:3995–4021.
[20] Laurent S, Forge D, Port M, Roch A, Robic C, Vander Elst L, et al. Magnetic iron oxide nanoparticles: synthesis, stabilization, vectorization, physicochemical characterizations, and biological applications. Chem Rev 2008;6:2064–110.
[21] Nelson GN, Roh JD, Mirensky TL, Wang Y, Yi T, Tellides G, et al. Initial evaluation of the use of USPIO cell labeling and noninvasive MR monitoring of human tissue-engineered vascular grafts in vivo. FASEB J 2008;22: 3888–95.
[22] Mertens ME, Frese J, Bölükbas DA, Hrdlicka L, Golombek S, Koch S, et al. FMN-coated fluorescent USPIO for cell labeling and non-invasive MR imaging in tissue engineering. Theranostics 2014;4:1002–13.
[23] Koch S, Flanagan TC, Sachweh JS, Tanios F, Schnoering H, Deichmann T, et al. Fibrin-polylactide-based tissue-engineered vascular graft in the arterial circulation. Biomaterials 2010;31:4731–9.
[24] Freed LE, Vunjak-Novakovic G, Biron RJ, Eagles DB, Lesnoy DC, Barlow SK, et al. Biodegradable polymer scaffolds for tissue engineering. Biotechnology 1994;12:689–93.
[25] Steinhoff G, Stock U, Karim N, Mertsching H, Timke A, Meliss RR, et al. Tissue engineering of pulmonary heart valves on allogenic acellular matrix conduits: in vivo restoration of valve tissue. Circulation 2000;102:III50–55.
[26] Mertens ME, Hermann A, Bühren A, Olde-Damink L, Möckel D, Gremse F, et al. Iron oxide-labeled collagen scaffolds for non-invasive MR imaging in tissue engineering. Adv Funct Mater 2014;24:754–62.